TECHNICAL REPORT ARCCB-TR-02012

DETRENDED FLUCTUATION ANALYSIS OF UV DEGRADATION IN A POLYURETHANE COATING

MARK A. JOHNSON
PAUL J. COTE

AUGUST 2002

US ARMY ARMAMENT RESEARCH,
DEVELOPMENT AND ENGINEERING CENTER
Close Combat Armaments Center
Benét Laboratories
Watervliet, NY 12189-4000

TACOM-ARDEC

20020913 105

DISCLAIMER

The findings in this report are not to be construed as an official Department of the Army position unless so designated by other authorized documents.

The use of trade name(s) and/or manufacturer(s) does not constitute an official endorsement or approval.

DESTRUCTION NOTICE

For classified documents, follow the procedures in DoD 5200.22-M, Industrial Security Manual, Section II-19, or DoD 5200.1-R, Information Security Program Regulation, Chapter IX.

For unclassified, limited documents, destroy by any method that will prevent disclosure of contents or reconstruction of the document.

For unclassified, unlimited documents, destroy when the report is no longer needed. Do not return it to the originator.

REPORT DOCUMENTATION PAGE

Public reporting burden for this collection of information is estimated to average 1 hour per response, including the time for reviewing instructions, searching existing data sources, gathering and maintaining the data needed, and completing and reviewing the collection of information. Send comments regarding this burden estimate or any other aspect of this collection of information, including suggestions for reducing this burden, to Washington Headquarters Services, Directorate for Information Operations and Reports, 1215 Jefferson Davis Highway, Suite 1204, Arlington, VA 22202-4302, and to the Office of Management and Budget, Paperwork Reduction Project (0704-0188), Washington, DC 20503.

1. AGENCY USE ONLY (*Leave Blank*)	2. REPORT DATE August 2002	3. REPORT TYPE AND DATES COVERED Final	

4. TITLE AND SUBTITLE
DETRENDED FLUCTUATION ANALYSIS OF UV .
DEGRADATION IN A POLYURETHANE COATING

5. FUNDING NUMBERS
AMCMS No. 6226.24.H180.0
PRON No. MIPR1PICTNY0

6. AUTHORS
Mark A. Johnson and Paul J. Cote

7. PERFORMING ORGANIZATION NAME(S) AND ADDRESS(ES)
U.S. Army ARDEC
Benet Laboratories, AMSTA-AR-CCB-O
Watervliet, NY 12189-4000

8. PERFORMING ORGANIZATION REPORT NUMBER
ARCCB-TR-02012

9. SPONSORING / MONITORING AGENCY NAME(S) AND ADDRESS(ES)
U.S. Army ARDEC
Close Combat Armaments Center
Picatinny Arsenal, NJ 07805-5000

10. SPONSORING / MONITORING AGENCY REPORT NUMBER

11. SUPPLEMENTARY NOTES
Submitted to *Journal of Coatings Technology.*

12a. DISTRIBUTION / AVAILABILITY STATEMENT
Approved for public release; distribution unlimited.

12b. DISTRIBUTION CODE

13. ABSTRACT *(Maximum 200 words)*

Changes in the intrinsic structure of paint surfaces resulting from extended UV exposure can significantly alter the appearance of the paint due to a breakdown in the resin that binds the fine paint particulates. In this study, the coating structure of a solvent-based polyurethane was analyzed to establish correlations between the intrinsic spatial scaling properties of the coating and UV exposure time. Atomic force microscopy (AFM) and laser scanning confocal microscopy (LSCM) were employed to map surface structures over a range of scales from 100-nm to 100-$\square$m. The roughness of the polyurethane surface was characterized in terms of scaling exponents by quantifying the local roughness using detrended fluctuation analysis (DFA) to identify long-range power-law correlations and correct for inhomogeneities in the surface structure. This approach provides a means to directly compare AFM and LSCM results over a range of scales consistent with those of a self-affine fractal. The time-dependent dynamics of the roughening process was also determined in order to provide a metric for characterizing the evolving surface morphology. The results provide fresh insight into the mechanisms of polyurethane coating degradation under UV exposure.

14. SUBJECT TERMS
Detrended Fluctuation Analysis, UV Degradation, Image Analysis, Fractals

15. NUMBER OF PAGES
15

16. PRICE CODE

17. SECURITY CLASSIFICATION OF REPORT UNCLASSIFIED	18. SECURITY CLASSIFICATION OF THIS PAGE UNCLASSIFIED	19. SECURITY CLASSIFICATION OF ABSTRACT UNCLASSIFIED	20. LIMITATION OF ABSTRACT UL

NSN 7540-01-280-5500

TABLE OF CONTENTS

TABLES

LIST OF ILLUSTRATIONS

INTRODUCTION

The surface morphology of a polyurethane coating is an important factor in determining a coating's appearance and properties. Extended UV exposure can alter this morphology by breaking down the resin that binds the fine paint particulates. Figure 1 shows scanning electron microscope (SEM) images illustrating the effect of UV exposure on a polyurethane coating. The figure shows the resin degradation that changes the appearance of the polyurethane coating under ambient light. There are two major effects of resin on appearance. First, the relative amount of resin in the paint controls the degree of gloss. Second, the resin serves to promote a uniform index of refraction throughout the filler particle/resin system in order to provide sufficient transparency so that the dye particles are observable. Resin degradation can thus affect appearance by altering the surface gloss through surface roughening and by promoting scatter from the loosened particles. Both factors can contribute to the UV fading (lightening) effect observed under ambient light for the solvent-based polyurethane employed in the present study. However, a UV-exposed polyurethane coating appears darker than an unexposed coating when both surfaces are coated with a conductive metal.
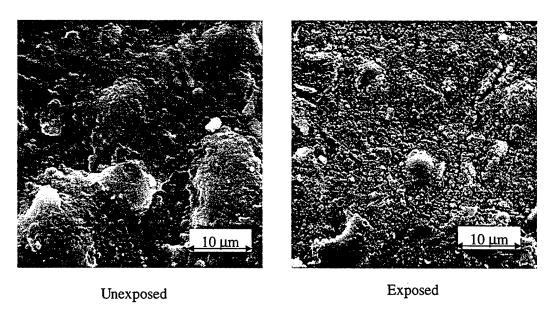

Unexposed

Exposed

Figure 1. Scanning electron microscope images of a polyurethane coating before and after 18 weeks of accelerated UV exposure.

Laser scanning confocal microscopy (LSCM) and atomic force microscopy (AFM) have been used for measures of specific paint surface features (refs 1,2). In the present study, LSCM and AFM were applied to quantify surface structures in terms of scaling properties. More specifically, the coating structure of the polyurethane paint surface was analyzed to establish correlations between the intrinsic spatial scaling properties of the surface and UV exposure time. The surface was analyzed as self-affine structure with statistical invariance under anisotropic dilations from the 10-μm AFM to the 100-μm LSCM scan sizes employed in the measurements. The scaling exponents that characterize a self-affine surface (ref 3) were initially determined using the height-height correlation function. However, inhomogeneities in the surface structure, variations in the curvature of the sample, and contributions from dominant features of the

1

substrate have a significant effect on this type of analysis. The effect is most noticeable in the analysis of the AFM images, where the curvature of the particles introduces inherent bias in the data. The influence of these effects can be minimized by analyzing the surface relative to a curved-reference surface (refs 4,5) or dividing the surface into patches that are analyzed separately using the "min-max" method (ref 6). Meisel et al. (ref 4) suggest a technique for measuring scaling properties relative to a curved-reference surface by limiting analysis to local, statistically homogenous regions that are large enough to define a statistically reliable height-height correlation function. However, determining the size of the regions that properly adapt to the heterogeneity of the surface requires subjective investigator input. The "min-max" method requires the investigator to judge the number of local maxima and minima of the surface to use in the analysis. A DFA does not require subjective input and is a systematic procedure that is well suited for measuring the subtle changes in scaling exponents of paint surfaces that result from UV exposure.

Peng et al. (ref 7) introduced DFA to determine long-term correlations embedded in time-series data. The sequence of integrated data of length N is divided into N/l nonoverlapping segments of length l. The average local variance of the segments is measured relative to a linear least-squares fit to the data within each segment l. The dependence of the variance on l defines the scaling properties of the time-series.

APPROACH

In the present study, DFA was used to determine the scaling properties of surfaces in three-space using spatial averages of roughness for surface patches of width l measured relative to a plane-fit (Appendix A) to the local data. The average local roughness, $w_L(l,t)$, is given by

$$w_L^2(l,t) \equiv \left\langle [h(x,t) - h_l(x,t)]^2 \right\rangle_x \tag{1}$$

where $h(x,t)$ is the height of a single-valued surface at location x relative to a plane-fit to the local data at time t, $h_l(x,t)$ is the average height of the local data at time t, t is the exposure time, and l is the size of local surface patches. $w_L(l,t)$ is measured for geometrically increasing values of l ($l <$ system size L) for each exposure time t. The dependence of the local roughness on l gives rise to the scaling properties of the fluctuations characterized by the roughness exponent α at time t as (ref 8)

$$w_L(l,t) \sim l^{\alpha} \tag{2}$$

Figure 2 shows filtered LSCM data and the patchwork of local reference surfaces employed by DFA for $l = 1.25$, 2.5, and 5.0-μm. The system size (scan size) is $L = 10$-μm for the AFM data and $L = 100$-μm for the LSCM data.
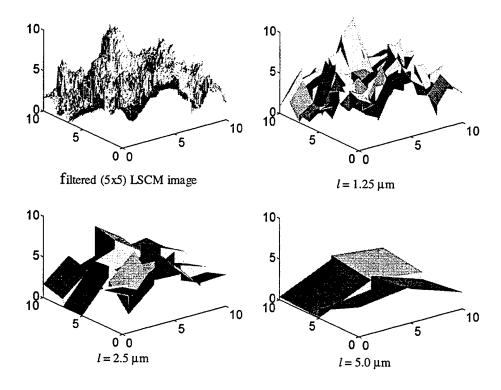
2

Figure 2. DFA reference patches for a 10-μm filtered LSCM image
of a solvent-based polyurethane. (All dimensions in μm.)

The paint in the present study is a solvent-based polyurethane system (MIL-PRF-85285) using nonpolymeric flattening agents (silica), and is pigmented to Air Force gray color number 37375. The accelerated coating degradation was conducted using a QUV weathering chamber according to test method ASTM G 53-96. A UVA 340 light source was used that emitted a spectral irradiance of 0.77 W/m^2 measured at 340-nm.

The time evolution for each of the exposed paint surfaces is not available, however, samples are available for three different UV exposure times. The DFA for these samples indicates that $w_L(l,t)$ does not saturate at the maximum exposure time. Therefore, the time evolution of the intrinsic surface structure as a function of UV exposure time was measured in terms of the growth exponent, β (ref 6). β characterizes the time-dependent dynamics of the roughening process for times much less than a saturation time, t_x, as

$$w_L(l,t) \sim t^\beta \qquad (t \ll t_x) \qquad (3)$$

Both LSCM and AFM were employed to map surface structure on a scale from 100-nm to 100-μm. These techniques generate surfaces in three-space that quantify surface morphology with little or no sample preparation. The AFM is a type of scanning probe microscopy that provides high-resolution images by scanning a sharp probe (2-nm to 20-nm tip radius) mounted on a flexible cantilever across a surface. A laser is focused on the tip and the beam is reflected

3

back to a photodiode. Deflections in the cantilever are measured at the photodiode and recorded as the tip scans across the surface. The AFM images in this investigation have a 20-nm horizontal resolution and a 0.1-nm vertical resolution.

The LSCM is an optical technique that generates a surface three-space using a series of two-dimensional images collected sequentially. Each two-dimensional image represents the measured reflected intensity of a laser-scanning beam focused on a matrix of points in a single focal plane. The focal plane is changed incrementally and the height of the surface at each point in the matrix is given by the maximum value of each two-dimensional image at that point. The wavelength of light and the numerical aperture of the lens limit the lateral resolution. The LSCM images in this investigation have a 0.25-μm lateral resolution and a 0.1-μm vertical resolution (ref 9).

An inherent limitation of practical LSCM is the contamination of images with noise spikes. These spikes are a result of low surface reflectivity, the objective lens, and edge effects of the surface. They are a consequence of associating noise on a low-level signal with the maximum reflected intensity at a given focal plane. The height at a given location directly correlates with the maximum intensity of the reflected laser detected by the photodiode, which is assumed to be at the appropriate focal plane. However, the intensity of the reflected beam may remain low at a given point in the two-dimensional matrix for the entire series of focal planes in the scan (usually 256). In this case, the height recorded at that point may correspond to a noise signal that is a maximum at any of the focal planes during the scan. The low intensity of the reflected beam can result from the inability of the scanning beam to properly focus on edges of surface inhomogeneities. This effect introduces spurious spikes around such edges. Our results suggest that as the complexity of a surface increases, there is a proportional increase in the density of this spike noise.

RESULTS

Inspection of these specimens under ambient light shows the familiar feature that alterations in surface appearance vary directly with UV exposure time. Quantitative measurements of reflectivity properties are in progress. The as-deposited paint color is medium gloss, light gray, which becomes significantly whiter in color under ambient light with UV exposure time. By contrast, the specimens sputter coated with palladium show the reverse effect in that the UV exposed specimens darken under ambient light relative to an unexposed palladium-coated paint specimen. The following results relate directly to the origin of these appearance changes. All quantitative measures represent averages of five different scans for exposed surfaces and fifteen different scans for unexposed surfaces.

Figure 3 is a comparison of 10-μm AFM and LSCM images (filtered and unfiltered) of a typical paint surface. The figure also shows the results of filtering the LSCM data with a nonlinear median filter using different size convolution kernels. The median filter is well suited for removing the spike noise associated with LSCM images, since edge information is preserved. The paint surfaces shown in Figure 3 were coated with 60-nm of sputtered palladium to prevent the LSCM scanning laser from penetrating the paint surface and ensure the images represent the same surface topology as measured by the AFM. The sputtered-palladium process is expected to

accurately replicate the substrate for these substrates. A DFA study of AFM images has shown that 60-nm of sputtered palladium has no detectable effect on the surface morphology. Figure 4 shows a comparison of the coated and uncoated LSCM DFA results for exposed and unexposed surfaces using 5x5 median filtering. The results show the optical surface (uncoated) generated by the LSCM relative to the actual physical surface (coated). The maximum difference between the physical surface and the optical surface is near the 0.1-µm LSCM resolution.

AFM image   raw LSCM image

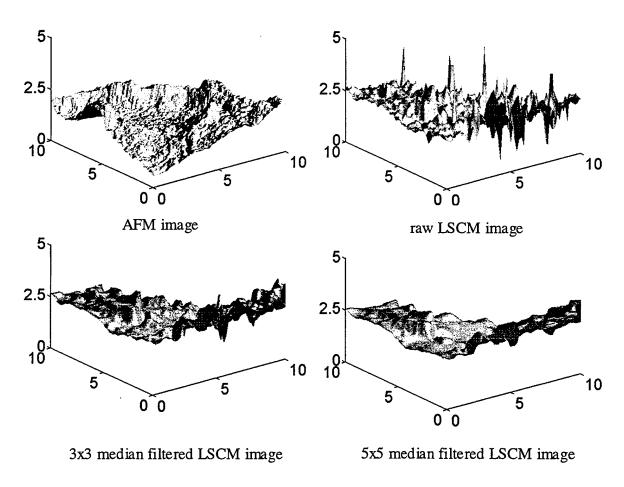3x3 median filtered LSCM image   5x5 median filtered LSCM image

Figure 3. Baseline 10-µm AFM and LSCM raw and filtered images of a coated, unexposed solvent-based polyurethane. (All dimensions are in µm.)
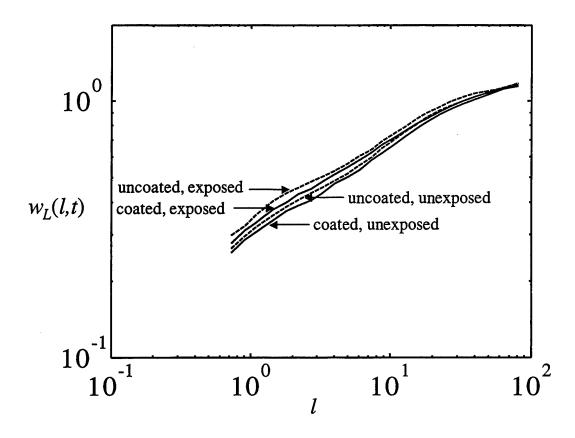
Figure 4. DFA results for LSCM images of uncoated and coated paint
samples using 5x5 median filtering. (All dimensions are in μm.)

In addition to providing a means for measuring the scaling properties of an
inhomogeneous surface structure, DFA was also used to determine the appropriate technique for
minimizing the considerable effects of the noise associated with LSCM images. Figure 5 shows
the results of DFA applied to AFM and LSCM data sets collected from a palladium-coated
sample with 18 weeks of UV exposure. A DFA was employed to determine the optimal filter for
removing surface artifacts from LSCM images. The DFA results are shown for raw AFM and
LSCM data and for the LSCM data after median filtering with different size convolution kernels.
The 10-μm images shown in Figure 3 suggest that LSCM data that have been filtered with a
nonlinear median filter are consistent with the baseline AFM image considering the lower
resolution of the LSCM data. The DFA results given in Figure 5 show that median filtering of
LSCM data with a 5x5 or 7x7 convolution kernel is the best compromise in ensuring that the
LSCM data are consistent with AFM results. To minimize the effect of offset in w_L that can
occur while acquiring AFM and LSCM images, the difference in DFA results $((w_L(l,t)^2 -
w_L(l,t_0)^2)^{1/2})$ between 18-week and unexposed paint surfaces was also computed to aid in
selecting the appropriate filter. Figure 6 shows these results for different size convolution
kernels. The results suggest that median filtering of LSCM images with a 5x5 convolution
kernel produces results consistent with the baseline AFM data. Therefore, a 5x5 median filter
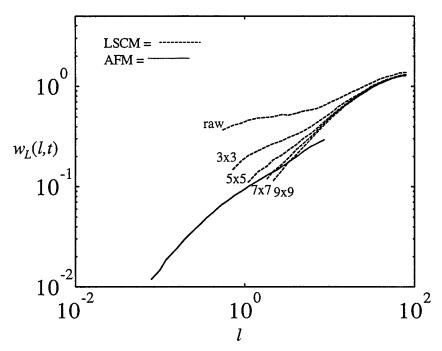was applied to all of the 10-μm LSCM images in this study.

6

Figure 5. Local scaling for coated samples after 18 weeks of exposure. Results are shown for unfiltered AFM images and for filtered LSCM images with different size convolution kernels. (All dimensions are in μm.)
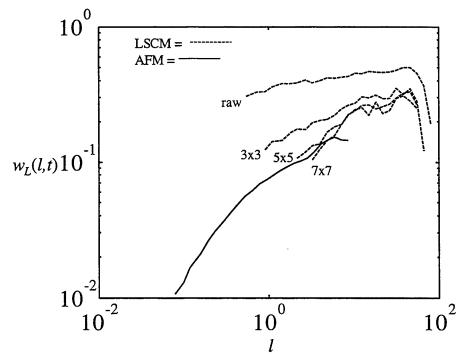

Figure 6. Difference in local scaling between coated samples after 18 weeks of exposure and coated unexposed samples. Results are shown for the unfiltered AFM images and for filtered LSCM images with different size convolution kernels. (All dimensions are in μm.)

7

Figure 7 shows the results of DFA applied to filtered LSCM images of unexposed surfaces and for surfaces after 3, 6, and 18 weeks of UV exposure. The effects of UV exposure are greatest at small $l(< 5$-μm) and have no discernable effect on the surface morphology for $l >$ 10-μm. The results also show that a single exponent cannot adequately describe the scaling behavior of the surfaces. Therefore, we employed a new procedure to determine if this type of coating structure is consistent with bimodal behavior having two unique scaling regions, and to obtain accurate measures of the two regions. We developed this technique to introduce a systematic method for extracting the scaling parameters, since there is no universally agreed upon procedure for estimating the exponent values, and blind regression fits to the height correlation data result in misleading values in the exponent (ref 6). This technique determines the scaling parameters by fitting two linear and one polynomial spline to the DFA results and estimating the scaling measures using the data that minimize the residuals in the fit (ref 10). The procedure is summarized in Appendix B. The bimodal fit to the data resulted in scaling regions between approximately 1.5 to 6-μm and between 5 and 15-μm. Analysis was limited to the 1.5 to 5-μm, where $w_L(l,t)$ increases with UV exposure time. Beyond 6-μm, DFA results overlap and no significant effects of UV exposure are evident.
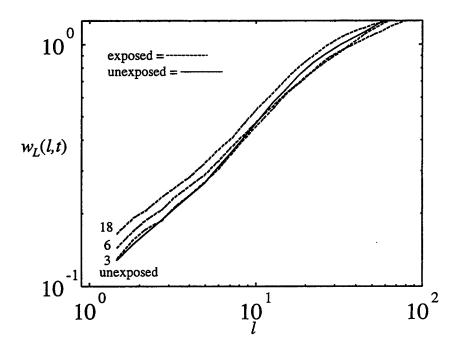

Figure 7. Local scaling of uncoated, filtered, 10-μm LSCM images of a solvent-based polyurethane with increasing UV exposure. (All dimensions are in μm.)

8

Table 1 summarizes the results of the bimodal analysis. The roughness of the surface on the 1.5 to 6-μm scale increases (α decreases) monotonically with increased exposure time. Figure 7 shows that $w_L(l,t)$ does not saturate with time, therefore, the growth exponent, β, was measured by analyzing the time evolution of the surface assuming times shorter than the saturation crossover time, t_x. β was determined using unfiltered data by assuming that spike noise is proportional to surface roughness. The time evolution $w_L(l,t)$ was measured relative to $w_L(l,0)$ (variances of uncorrelated data are additive), which is nonzero for the unexposed surface. β was determined for values of l up to the limit of the first scaling region (6-μm) and the results averaged, assuming a fixed α. This ensured the evolution of roughness was a function of UV exposure time only. The time evolution of the surface described by β was determined to be 0.25 ±0.02.

Table 1. Bimodal Analysis

Exposure Time (Weeks)	First Scaling Region (μm)	Second Scaling Region (μm)	α
0	1.5 to 5	5 to 15	0.60
3	1.5 to 6	6 to 9	0.58
6	1.5 to 5	5 to 13	0.56
18	1.5 to 6	5 to 15	0.53

DISCUSSION and CONCLUSIONS

The results in Figures 4 through 7 show that there is generally a spectrum of local roughness values to consider when quantifying the effect of UV exposure on the structure of the paint. The surface structure of the solvent-based polyurethane paint in this study changes with UV exposure, but only by small amounts (< 0.15-μm) and at very small scales (< 6-μm). The appearance of the polyurethane coating under ambient light changes (i.e., becomes lighter) due to a breakdown in the resin that binds the fine particulates. The absence of flattening additives in the paint suggests that the appearance changes originate primarily from surface roughness changes. The corresponding results for palladium-coated specimens, where light penetration is precluded, show that light scattering associated with UV-induced roughness changes produces significant darkening. This illustrates that both subsurface effects and surface roughness contribute to appearance changes associated with UV exposure.

The resolution of LSCM images is adequate for measuring general changes in surface morphology of the paints; however, inherent noise at scales in the range of interest must be removed. Using AFM provides essential reference data for determining the best technique for removing this noise. A single growth exponent, β, can describe the time-dependent dynamics of the UV-induced roughening process assuming LSCM spike noise varies directly with surface roughness.

9

Detrended fluctuation analysis is a valuable, systematic technique for obtaining the scaling exponents of an inhomogeneous structure. It is particularly convenient when analyzing real data for scaling properties where the underlying background structure is a dominant factor in the measurements. In the present study, DFA provided a means for quantifying the subtle changes that occur in surface morphology as the resin deteriorates under UV exposure. The intrinsic structure of the paint in this study is consistent with a self-affine surface fractal having two distinct scaling regions. Only the small scaling region is affected by UV exposure, and increases in complexity with time.

SUMMARY

Changes in the intrinsic structure of paint surfaces resulting from extended UV exposure can significantly alter the appearance of the paint due to a breakdown in the resin that binds the fine paint particulates. These changes were characterized in terms of scaling exponents by quantifying the local roughness using DFA to identify long-range power-law correlations and correct for inhomogeneities in the surface structure. The DFA was shown to provide a valuable, systematic technique for obtaining the scaling exponents of an inhomogeneous structure. It was particularly convenient for the paints in this study where the underlying background structure was a dominant factor in the measurements. The complexity of the surface was shown to increase monotonically with UV exposure time, and the dynamics of this roughening process was described by a single scaling exponent.

REFERENCES

1. Sung, L., Nadal, M.E., McKnight, M., Marx, E., and Laurenti, B., "Optica Reflectance of Metallic Coatings: Effect of Aluminum Flake Orientation," submitted to *Journal of Coatings Technology,* to be published.

2. Hegedus, C.R., and Kloiber, K.A., "Aqueous Acrylic-Polyurethane Hybrid Dispersions and Their Use in Industrial Coatings," *Journal of Coatings Technology*, Vol. 68, 1996.

3. Gouyet, J.F., Rosso, M., and Sapoval, B., *Fractals and Disordered Systems*, (A. Bunde and S. Havlin, Eds.), Springer, Berlin, 1991, pp. 229-234.

4. Meisel, L.V., Scanlon, R.D., Johnson, M.A., and Lanzerotti, Y.D., "Self-Affine Analysis on Curved Reference Surfaces: Self-Affine Fractal Characterization of TNT Fracture Surface," *Shock Compression of Condensed Matter*, Vol. 1, 1999, pp. 727-730.

5. Cote, P.J., and Johnson, M.A.,"Self-Affine Scaling Analysis of Coating Structure," *Proceedings of the SPIE Visual and Information Processing Conference*, Vol. 3716, 1999, pp. 2-8.

6. Peng, C.K., Buldyrev, S.V., Goldberger, A.L., Havlin, S., Sciortino, F., Simons, M., and Stanley, H.E., "Long-Range Correlations in Nucleotide Sequences," *Nature*, Vol. 356, 1992, pp. 168-171.

7. Peng, C.K., Buldyrev, S.V., Havlin, S., Simons, M., Stanley, H.E., and Goldberger, A.L., "Mosaic Organization of DNA Nucleotides," *Physical Review E*, Vol. 49, No. 2, 1994, pp. 1685-1688.

8. Barabasi, A.L., and Stanley, H.E., *Fractal Concepts in Surface Growth*, Cambridge University Press, 1995.

9. *Confocal Laser Scanning Microscope, 1LM21*, Operations Manual, No. 4B-3601, Lasertec Corporation.

10. Johnson, M.A., and Cote, P.J., "Characterization of Metastable Structures in Sputtered Coatings," *Proceedings of the Systemics, Cybernetics, and Informatics Conference*, Vol. 6, 2001, pp. 298-303.

APPENDIX A

The following series of equations provides the coefficients of a plane-fit ($f(x,y) = a + bx + cy$) to the data z_i that minimize the square of the residuals ($\varepsilon_i = a + bx_i + cy_i - z_i)^2$ for all points, m, containing a local surface patch of length l:

$$\frac{\partial S}{\partial a} = 0 \Rightarrow a * m + b\sum_1^m x_i + c\sum_1^m y_i = \sum_1^m z_i \tag{A1}$$

$$\frac{\partial S}{\partial b} = 0 \Rightarrow a\sum_1^m x_i + b\sum_1^m x_i^2 + c\sum_1^m x_i y_i = \sum_1^m x_i z_i \tag{A2}$$

$$\frac{\partial S}{\partial c} = 0 \Rightarrow a\sum_1^m y_i + b\sum_1^m x_i y_i + c\sum_1^m y_i^2 = \sum_1^m y_i z_i \tag{A3}$$

APPENDIX B

A new systematic procedure was developed to determine if a distribution exhibits bimodal behavior and to obtain accurate measures of the two scaling regions. The technique determines the scaling parameters by fitting a two-linear and one-polynomial spline to the data and estimating the scaling measures using the data that minimize the residuals in the fit. The first linear range is determined by fitting a straight line, f_1, to the first k_1 points, and the second linear region is determined by fitting a straight line, f_2, to the second k_2 points. A polynomial, f_3, is then fit to points k_2 through m, where m is the last point in the fit of f_3. k_1 is the index of the data point at which the two linear regions meet, and k_2 is the index of the data point at which f_2 and f_3 join. Both k_1 and k_2 are variable knots (indices) of a linear/linear and a linear/curved spline and are nonlinear parameters determined by exhaustion. The coefficients of the polynomials are evaluated with continuity enforced at k_1 and k_2, and the residuals (ε_i) are computed over the entire range. The values of k_1 and k_2 for which the residuals are a minimum are selected as the indices for the knots. The shape of the height correlation data suggests that a quadratic fit is sufficient to determine k_2, although the procedure is similar if higher order polynomials for f_3 are used. Continuity is enforced for both knots with additional C^1 continuity enforced for the quadratic fit at k_2. If either f_1 or f_2 are determined to have fewer than three points, then it is assumed that only one linear region exists and the structure is not bimodal. If both f_1 and f_2 have fewer than three points, then no linear region exists. If the structure is determined to be bimodal, k_1 is assumed to be the limit of the first scaling range. k_2 is determined from the intersection of f_2 and the saturation limit where no correlation is observed. The procedure is outlined below as

$$f_1(x) = a + b(x - k_1) \qquad \text{(B1)}$$

$$f_2(x) = c + d(x - k_1) \qquad \text{(B2)}$$

$$f_3(x) = e + f(x - k_2) + g(x - k_2)^2 \qquad \text{(B3)}$$

Assuming continuity at knots k_1 and k_2, with additional C^1 continuity at k_2,

$$f_1(k_1) = f_2(k_1), \ f_2(k_2) = f_3(k_2), \ f_2'(k_2) = f_3'(k_2) \qquad \text{(B4)}$$

and the residuals (ε_i) become

$$\varepsilon_i = a + bp_{i1} - y_i, \quad for \ i < k_1$$

$$\varepsilon_i = a + dp_{i1} - y_i, \quad for \ k_1 < i \leq k_2$$

$$\varepsilon_i = a + d(K + p_{i2}) + g(q_{i2}) - y_i, \quad for \ k_2 < i \leq m$$

where

$$p_{i1} = x_i\text{-}k_1, \quad q_{i1} = (x_i\text{-}k_1)^2, \quad p_{i2} = x_i\text{-}k_2, \quad q_{i2} = (x_i\text{-}k_2)^2 \tag{B5}$$

and y_i is the measured value at i.

The coefficients of the polynomials are determined by minimizing the sum of the squares of the residuals S

$$S = \sum_1^m \varepsilon_i^2 = \sum_1^{k_1} \varepsilon_i^2 + \sum_{k_1+1}^{k_2} \varepsilon_i^2 + \sum_{k_2+1}^m \varepsilon_i^2 \tag{B6}$$

$$\frac{\partial S}{\partial a} = 0 \Rightarrow a*m + b\sum_1^{k_1} p_{i1} + d\sum_{k_1+1}^{k_2} p_{i1} + d\left[\sum_{k_2+1}^m p_{i2} + KA\right] + g\sum_{k_2+1}^m q_{i2} = \sum_1^m y_i \tag{B7}$$

$$\frac{\partial S}{\partial b} = 0 \Rightarrow a\sum_1^{k_1} p_{i1} + b\sum_1^{k_1} q_{i1} = \sum_1^{k_1} y_i p_{i1} \tag{B8}$$

$$\frac{\partial S}{\partial d} = 0 \Rightarrow a\left[\sum_{k_1+1}^{k_2} p_{i1} + \sum_{k_2+1}^m p_{i2} + KA\right] + d\left[\sum_{k_1+1}^{k_2} q_{i1} + 2K\sum_{k_2+1}^m (p_{i2}+q_{i2}) + K^2A\right] +$$

$$g\left[\sum_{k_2+1}^m q_{i2}(K+p_{i2})\right] = \sum_{k_1+1}^{k_2} y_i p_{i1} + \sum_{k_2+1}^m y_i(K+p_{i2}) \tag{B9}$$

$$\frac{\partial S}{\partial g} = 0 \Rightarrow a\sum_{k_2+1}^m q_{i2} + d\left[\sum_{k_2+1}^m q_{i2}(K+p_{i2})\right] + g\sum_{k_2+1}^m q_{i2}^2 = \sum_{k_2+1}^m y_i q_{i2} \tag{B10}$$

where $K = x(k_2)\text{-}x(k_1)$, and $A = m\text{-}k_2$.

14

TECHNICAL REPORT INTERNAL DISTRIBUTION LIST

	NO. OF COPIES
TECHNICAL LIBRARY ATTN: AMSTA-AR-CCB-O	5
TECHNICAL PUBLICATIONS & EDITING SECTION ATTN: AMSTA-AR-CCB-O	3
OPERATIONS DIRECTORATE ATTN: SIOWV-ODP-P	1
DIRECTOR, PROCUREMENT & CONTRACTING DIRECTORATE ATTN: SIOWV-PP	1
DIRECTOR, PRODUCT ASSURANCE & TEST DIRECTORATE ATTN: SIOWV-QA	1

NOTE: PLEASE NOTIFY DIRECTOR, BENÉT LABORATORIES, ATTN: AMSTA-AR-CCB-O OF ADDRESS CHANGES.

TECHNICAL REPORT EXTERNAL DISTRIBUTION LIST

	NO. OF COPIES		NO. OF COPIES
DEFENSE TECHNICAL INFO CENTER ATTN: DTIC-OCA (ACQUISITIONS) 8725 JOHN J. KINGMAN ROAD STE 0944 FT. BELVOIR, VA 22060-6218	2	COMMANDER ROCK ISLAND ARSENAL ATTN: SIORI-SEM-L ROCK ISLAND, IL 61299-5001	1

COMMANDER
U.S. ARMY ARDEC
ATTN: AMSTA-AR-WEE, BLDG. 3022
     AMSTA-AR-AET-O, BLDG. 183
     AMSTA-AR-FSA, BLDG. 61
     AMSTA-AR-FSX
     AMSTA-AR-FSA-M, BLDG. 61 SO
     AMSTA-AR-WEL-TL, BLDG. 59
PICATINNY ARSENAL, NJ 07806-5000
	1
	1
	1
	1
	1
	2
		COMMANDER
		U.S. ARMY TANK-AUTMV R&D COMMAND
		ATTN: AMSTA-DDL (TECH LIBRARY)
		WARREN, MI 48397-5000
			1

DIRECTOR U.S. ARMY RESEARCH LABORATORY ATTN: AMSRL-DD-T, BLDG. 305 ABERDEEN PROVING GROUND, MD 21005-5066	1	COMMANDER U.S. MILITARY ACADEMY ATTN: DEPT OF CIVIL & MECH ENGR WEST POINT, NY 10966-1792	1
DIRECTOR U.S. ARMY RESEARCH LABORATORY ATTN: AMSRL-WM-MB (DR. B. BURNS) ABERDEEN PROVING GROUND, MD 21005-5066	1	U.S. ARMY AVIATION AND MISSILE COM REDSTONE SCIENTIFIC INFO CENTER ATTN: AMSAM-RD-OB-R (DOCUMENTS) REDSTONE ARSENAL, AL 35898-5000	2
COMMANDER U.S. ARMY RESEARCH OFFICE ATTN: TECHNICAL LIBRARIAN P.O. BOX 12211 4300 S. MIAMI BOULEVARD RESEARCH TRIANGLE PARK, NC 27709-2211	1	COMMANDER U.S. ARMY FOREIGN SCI & TECH CENTER ATTN: DRXST-SD 220 7TH STREET, N.E. CHARLOTTESVILLE, VA 22901	1

NOTE: PLEASE NOTIFY COMMANDER, ARMAMENT RESEARCH, DEVELOPMENT, AND ENGINEERING CENTER,
BENÉT LABORATORIES, CCAC, U.S. ARMY TANK-AUTOMOTIVE AND ARMAMENTS COMMAND,
     AMSTA-AR-CCB-O, WATERVLIET, NY 12189-4050 OF ADDRESS CHANGES.